IEEE Access
Multidisciplinary ⋮ Rapid Review ⋮ Open Access Journal

Received June 3, 2021, accepted June 18, 2021, date of publication June 23, 2021, date of current version July 1, 2021.

Digital Object Identifier 10.1109/ACCESS.2021.3091772

Upscaling Strategy to Simulate Permeability in a Carbonate Sample Using Machine Learning and 3D Printing

MOHAMED SOUFIANE JOUINI[1], JORGE SALGADO GOMES[2], MOUSSA TEMBELY[3], AND EZDEEN RAED IBRAHIM[4]

[1]Department of Mathematics, Khalifa University, Abu Dhabi, United Arab Emirates
[2]Subsurface Excellence Division, Abu Dhabi National Oil Company, Abu Dhabi, United Arab Emirates
[3]Department of Petroleum Engineering, Khalifa University, Abu Dhabi, United Arab Emirates
[4]Department of Petroleum Geosciences, Khalifa University, Abu Dhabi, United Arab Emirates

Corresponding author: Mohamed Soufiane Jouini (mohamed.jouini@ku.ac.ae)

This work was supported in part by the Abu Dhabi Department of Education and Knowledge (ADEK) in United Arab Emirates under Grant EX2018-024 for the research project "Simulation and validation of oilfield reservoir rock properties using 3D-printing and machine learning."

ABSTRACT Characterizing heterogeneity is crucial to assess the variability of rock properties in carbonate reservoir samples. This work introduces an original multiscale approach to simulate permeability and porosity in heterogeneous carbonate samples using 3D X-ray computed tomography images. The main novelty of our approach is to introduce a quantitative heterogeneity description in terms of texture classification using machine learning. The rock texture classification result is then used to upscale rock properties simulations from fine to coarse scale. The fine scale properties are investigated based lattice Boltzmann method, while a Darcy-scale flow simulator is adopted for estimating coarse scale properties. In addition, due to the critical role played by petrophysical properties at fine scale, a 3D printing technique is employed to validate experimentally the numerical simulations at this scale. Finally, we present an application of our proposed approach on a real carbonate sample from the Middle East carbonate oilfield reservoir.

INDEX TERMS Machine learning, micro-computed tomography, permeability, upscaling, 3D printing.

I. INTRODUCTION

Characterizing accurately rock properties at core scale is critical for reservoir scale modeling. This step is especially complex when dealing with carbonate rocks because of their inherent heterogeneities at several length scales. Indeed, deposition and diagenesis produce heterogeneous pore-shaped geometries that may have a significant impact on petrophysical properties [1], [2]. For example, two core plug samples extracted from adjacent locations in a carbonate core may have significantly different rock properties. Standard core analysis methods provide accurate experimental laboratory measurements. However, these techniques do not take into account the pore-scale variability inside core plug samples. Digital rock physics (DRP) is an approach that aims to characterize rock properties at pore scale by acquiring rock samples using X-ray micro-tomography and numerical simulation methods [3]–[9]. DRP has been largely used to estimate several rock properties, such as porosity, permeability and elastic moduli, in siliciclastics and carbonate rocks. However, a clear workflow to numerically characterize rock properties in carbonates is lacking [10]–[12].

The general strategy to deal with heterogeneity is to apply a multiscale imaging approach, which first involves scanning a core plug sample at a coarse-scale (15 to 20 μm) resolution. This first acquisition provides a general idea about textures variability inside the core plug sample. The second step is the physical extraction of small subsets from representative homogeneous zones, which are scanned at a fine scale (1-4 μm) to reveal pore structures. The third step is the execution of numerical simulations to estimate rock properties on the fine-scale digital models. Finally, simulated rock properties are up-scaled from fine to coarse scale in order to obtain the effective property. Over the years, several multiscale imaging and simulation studies have investigated the up-scaling of carbonate rocks properties. Some authors

The associate editor coordinating the review of this manuscript and approving it for publication was Hiu Yung Wong.

implemented a classical strategy to deal with simulations at different length scales using a representative volume element procedure. This approach did not succeed in modeling rock properties in carbonate rocks, owing to their high heterogeneity [4], [12], [13]. Other authors simulated rock properties at fine scale and then implemented upscaling procedures to simulate properties at coarse scale. For example, Reference [14] used a correlation between FIBSEM and X-ray micro computed tomography grey levels images to successfully upscale porosity from fine to coarse scales in a carbonate sample. Other authors introduced a multiscale approach based on reconstructing the pore structure from fine-scale 2D scanned images of a carbonate sample to simulate absolute permeability at coarse scale [15]. Nevertheless, the reconstruction method was very sensitive and dependent on too many factors, including segmentation at several length scales, pore network extraction and stochastic network generation. Some researchers introduced an upscaling method based on correlating registered X-ray micro computed tomography images acquired at different resolutions to estimate the absolute permeability of carbonate samples [16]. The main idea consisted of first correlating simulated fine-scale porosity and permeability values. Then, the authors used averaging methods, such as harmonic, arithmetic, and geometric means in addition to Darcy's law, to upscale permeability at coarse scale. Reference [17] proposed a workflow for porosity-permeability trends, upscaling based on DRP. The workflow proposed to integrate information between fine and coarse scales by extracting some statistics derived from a three-dimensional (3D) coarse-scale image and fine-scale permeability trends to produce the effective simulated properties. Results suggested up to a 50% error in permeability prediction for the proposed workflow. More recently, Reference [18] implemented a multi-scale approach that combined micro- and macro-scales simulations of absolute permeability and compared them with laboratory experiments for two carbonate samples. The authors implemented the lattice Boltzmann method (LBM) to perform micro-scale computations on subsets of images at fine scale. The result was used to determine the permeability and extract porosity-permeability trends. Then, images were registered between fine and coarse scales. Finally, a macro-scale computational grid was set to calculate porosity and permeability values at coarse scale. Although the authors obtained promising results on real carbonate samples, the proposed method is very sensitive to the manual selection of subset location and to the quality of the registration method applied between scales. More recently, a study was conducted using multiscale imaging and an upscaling approach with fractals. A fractal porosity equation was proposed, showing promising results only for porosity estimation in carbonate samples [19].

In most of these studies, two main common limitations can be observed in the implemented approaches. First, the proposed methodologies are not easily reproducible. Indeed, the selection of representative homogeneous textures regions for fine scale imaging is usually qualitative. The absence of a quantitative description of the core plug textures at coarse scale makes the up-scaled simulation result difficult to validate. In addition, in many cases, carbonate samples can reveal heterogeneous textures at several scales, requiring repeating the subjective qualitative selection procedure several times. The second limitation is the use of simulated rock properties at the finest scale, which cannot be validated experimentally in a laboratory. Indeed, extracted and scanned subsets sizes are in the range of a few millimeters, making it difficult to perform experimental laboratory measurements for permeability for example.

In this paper, we propose a novel upscaling approach to simulate porosity and absolute permeability in carbonate samples using texture classification. We introduce a quantitative textural description of core plug samples at several scales using texture analysis and classification through machine learning. In addition, we propose to use 3D printing technology as a tool to validate experimentally the rock properties simulations at fine scale.

Texture modeling has been widely implemented in the past decades for classification and segmentation purposes [7], [20], [21]. Texture applications are found in several areas of study, such as crystallography, stratigraphy, patterned fabrics and medical imaging [22], [23]. Texture modelling involves the analysis of an image by extracting a set of representative features, such as entropy, autocorrelation, uniformity, and Haralick's co-occurrence matrix [24]–[26]. In earth sciences applications, the concept of analyzing X-ray micro-computed tomography textures images to estimate rock properties has physical bases. Indeed, grey-level voxels are directly related to the density information of rock frame, which is revealed perceptually in X-ray images by the variations of granularity, mineralogy and porosity features). Reference [27] used a statistical texture model to relate elastic properties to textures of scanning acoustic microscope images of shale. Reference [28] implemented texture modeling to quantify and analyze anisotropy of grains orientations in some rock fabrics. Other authors proposed a textural parametric model to identify the main representative textures of X-ray-computed tomography images of cores extracted from a sandstone reservoir [7], [29].

Recently, advances in machine learning have revolutionized image processing applications. Convolutional neural networks (CNNs) are powerful tools suited to analyze textures, thanks to repetitive patterns that can be identified and learned through filter banks [7]. Recently, reference [32] proposed a specific architecture of CNNs called the U-Net architecture. This approach has been a widely used tool for segmentation in several applications, such as brain tumor detection, cell counting and subsurface facies modeling [30]–[32]. The U-Net architecture for the segmentation of textures was compared against several popular traditional segmentation strategies and the machine learning approach obtained the best texture classification result in standard texture databases [33].

In this study, we propose to implement the U-Net architecture to automatically classify X-ray micro computed image

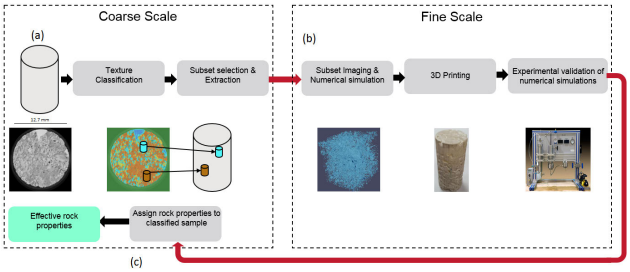

FIGURE 1. Multiscale procedure to simulate absolute permeability and porosity: a) At coarse scale we apply texture classification to target subset selection and extraction; b) At fine scale after scanning subsets, we simulate rock properties and print in 3D the magnified subset and measure experimentally rock properties of each subset; c) At coarse scale we assign rock properties simulated and validated experimentally to each texture to obtain the effective rock property.

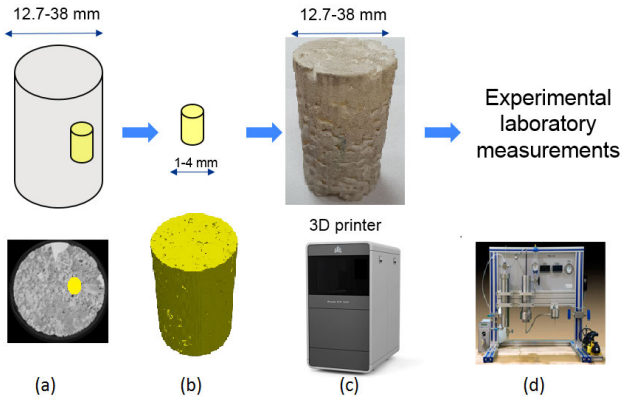

FIGURE 2. 3D printing workflow: a) Subset extracted and scanned at high resolution (1 to 4μm); b) Image segmentation and extraction of surface representing solid phase; c) 3D printing of surface by magnifying cylindrical sample to a diameter (12.7 to 38 mm); d) Laboratory measurements.

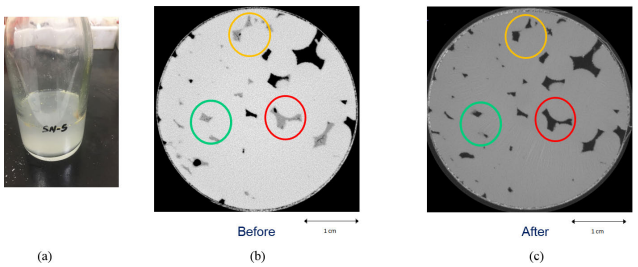

FIGURE 3. Cleaning 3D printed samples: a) The support material collected after the cleaning process at 80 degrees Celsius; b) X-Ray Micro computed tomography before cleaning: intermediate grey levels denote the support material trapped into the 3D printed sample; c) X-Ray Micro computed tomography after cleaning.

textures of carbonate rock samples. This automatic classification of carbonate textures images provides a quantitative criterion to describe texture variability. The approach helps to identify cubic subsets, which typically range in size between 1 mm to 4 mm, to be scanned at a high resolution corresponding to the fine scale. Then, we simulate numerically rock properties, at pore scale, using subsets of high resolution scanned images. We will implement LBM as numerical method to simulate permeability at subset scale. Indeed, several research studies proved that LBM could be a powerful tool to simulate absolute permeability in porous media [33], [34]. At the subset scale, experimental validation of numerical results is not possible because of technical limitations. We use 3D printing technology to overcome this disparity between experimental and numerical simulation scales.

Several research studies have used the 3D print representation of simple rock samples, obtained from X-ray micro-computed tomography images, to help understanding fluid flow behavior at pore scale. Reference [36] printed 3D synthetic representation of sandstone rock samples based on X-ray scanner at high resolution. The feasibility of the concept was proven by comparing numerical simulations of absolute permeability and experimental laboratory measurements. Reference [37] studied differences in porosity, permeability and mean pore throat radius between sandstone samples and upscaled 3D printed versions obtained from micro-computed tomography scans of real rock samples. We propose in this study a workflow to (i) implement 3D print synthetic representations for carbonates to validate the numerical approach, and (ii) to perform upscaling by combining texture analysis and machine learning (Figure 1).

II. MATERIALS AND METHODS

A. 3D PRINTING OF POROUS MEDIA

The available experimental laboratory devices for porosity and permeability measurements cannot be used for fine-scale subsets samples (1-4 mm). Thus, the subset size was magnified to a range of 12 to 38 mm so that experimental measurements could be carried out normally. This step aims to validate experimentally the numerical simulations used in our proposed upscaling workflow (Figure 2). The selected 3D printer Project MJP 3600 is based on stereolithography (SLA) technology. SLA is a variety of available 3D printing technologies that can produce models layer-by-layer using photochemical processes by which a laser beam solidifies chemical monomers to form polymers. In our study, the Project MJP 3600 used a photo-reactive resin to produce 3D samples with a resolution of 30 ìm per layer. The main input for the 3D printer is a digital model representing a 3D surface mesh of the solid phase. We obtained the solid phase by applying the bi-level segmentation method on each 3D X-ray micro-tomography image at fine scale [38]. The laser beam hardens the solid phase and keeps the soft resin as it is at the pore phase. The main challenge was removing the soft resin from the 3D printed sample cavities representing pore space. The 3D printed sample was heated to 80°C in an oven and then flushed with distilled water at 80°C and at a pressure range of 20-40 bars. The cleaning procedure took on average 10 to 12 days for most of the samples studied.

Figure 3.a illustrates the support material collected after the cleaning process. In addition, to check the performance of the cleaning process, we scanned printed samples before and after cleaning. Figure 3.b shows the soft resin trapped inside pores denoted with intermediate grey levels values before

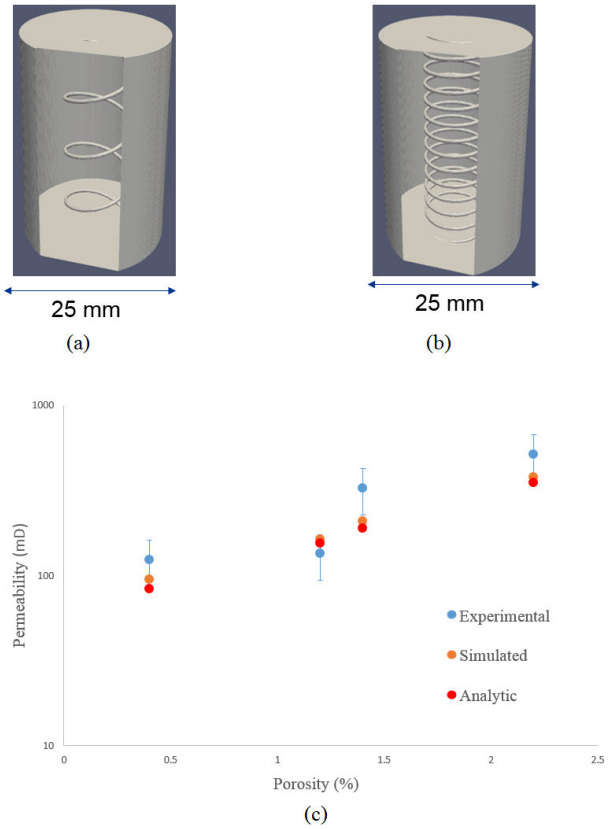

FIGURE 4. Synthetic digitally generated helical surfaces samples with 25 mm diameter: a) Tortuosity $\tau = 5$; b) Tortuosity $\tau = 18$, c) Comparison between analytic, numerical and experimental permeability values.

cleaning. Figure 3.c reveals the efficiency of the procedure at the same pores after cleaning. The next step was to measure experimentally the porosity and absolute permeability of the 3D printed samples and compare them to numerically simulated properties. We used VINCI Helium Porosimeter and VINCI Gasperm devices to measure the porosity and permeability. In order to validate the concept, we printed samples representing single helical tubes where analytical permeability values are available through (1):

$$K = \frac{\pi \cdot r^4}{8 \cdot A \cdot \tau} \tag{1}$$

where K is the permeability, A is the solid cylinder cross-sectional area, r is the helical tube radius and τ is the tortuosity.

Figure 4.a and Figure 4.b illustrate some digitally generated helical samples with variable tortuosity. To better characterize those 3D printed samples, we simulated the absolute permeability using LBM for each sample. Figure 4.c shows a comparison between simulated, experimental measurements and analytic solutions for the four synthetic samples. The porosity prediction aligned well with the measurements, confirming that most of the support material was successfully removed after the cleaning process. Experimental permeability values were also in the range of the analytic and simulated results (Table 1).

TABLE 1. Experimental and simulated porosity and permeability of 4 synthetic helical samples printed in 3D.

Sample	Porosity			Permeability		
	Size (mm)	Digital (%)	Experiment (%)	Analytic (mD)	LBM (mD)	Experiment (mD)
Helix 1	25	1	1.2	84	95	124
Helix 2	25	0.4	0.4	156	163	145
Helix 3	38	2.3	2.2	191	209	327
Helix 4	38	1.5	1.4	352	378	517

The deviation between experimental and analytical results can be explained by the printing resolution limitation. Indeed, for some samples, we generated helical tubes with radii corresponding to only five times the 3D printer resolution. At this level, the 3D printer may have produced a non-smooth tube surface causing a deviation from the digital input model. Thus, 3D printing can also be considered as an interesting tool assessing uncertainties at experimental level while measuring permeability. Based on these positive results, we printed more samples using X-ray micro-computed tomography of real rock images and applied the same cleaning process before measuring the porosity and permeability values. Results are reported and discussed in the Section IV of this paper.

B. TEXTURE CLASSIFICATION: U-NET

There are two main goals of using texture classification in this study. The first was to automatically identify the locations of representative textural subsets at fine scale. The second goal is to use the texture classification as a vector of continuity to bridge the gap between scales and predict the effective rock properties of carbonate samples. To achieve these goals, we implemented a supervised textural classification approach based on a machine learning method. Texture provides perceptually visual information about the spatial arrangement of intensities in an image. The supervised texture classification approach first involves establishing a list of a predefined representative textural classes based on user-visualization. Then, every analyzed pixel in the X-ray micro-computed tomography image is automatically assigned to a class. In the last decade, new image classification techniques have emerged based on machine learning and, more specially, the convolutional neural networks (CNN). Unlike standard texture classification approaches, this type of algorithm identifies content of images without the need for previous feature extraction. Indeed, thanks to the convolutional filters, this step is performed automatically at the training stage. In our study, we implemented the U-Net as a CNN method to perform texture classification.

The purpose of a CNN is to analyze the feature mapping of an image. In other words, images are transformed into vectors used for classification. More particularly, we implemented the U-Net architecture, a CNN that was originally developed for biomedical image classification applications [30]. The U-Net is a type of architecture that uses a fully convolutional network model implementing a network with successive layers including up-sampling and down-sampling operators. The

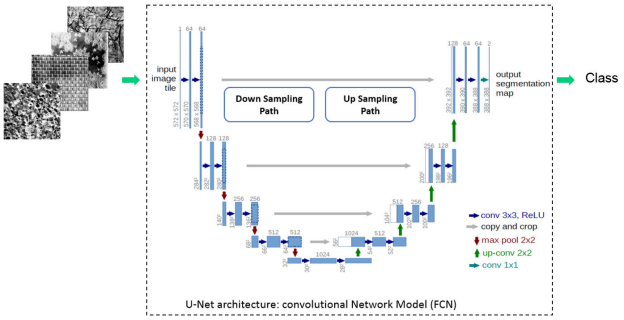

FIGURE 5. The general architecture of the U-Net convolutional network model. Input images are textures of 256 × 256 pixels and output are class numbers.

u-shaped architecture consists of a contracting path and an expansive path. The contracting path is a standard convolutional network implemented with repeated convolutions, after which each is followed by a rectified linear unit (ReLU) and a max pooling operation. The contraction path reduces the information while feature information is increased. Figure.5 illustrates the general architecture of the U-Net convolutional network model. The down-sampling path is a contractive path used to capture the context of the image. The basic principle for this path is to reduce the resolution of the image and to increase the depth corresponding to the number of layers with no padding. The path consists of four convolutional blocks (two convolution layers each with 3 × 3 filter with ReLU activation) followed by max-pooling layers 2 × 2 with stride 2 for down-sampling. The fifth convolution layer is without max pooling to make a connection to the up-sampling path.

The first convolutional block has 64 filters on each convolutional layer. The number of filters doubles with each consecutive convolutional block. The up-sampling path is a symmetric expanding path used for precise localization. The main goal of using the up-sampling map is to increase resolution and reduce the number of layers, or depth, with no padding. The pooling operators are replaced with up-sampling operators. Hence, these layers increase the resolution of the output. Similar to the down sampling path, the up-sampling path also consists of several expansion blocks. Each block passes through two 3 × 3 convolution layers, followed by a 2 × 2 up-sampling layer. The number of filters for each convolution block equals half of the filters from the previous convolutional block. The final layer is a 1 × 1 convolution used to map each 64-components feature vector to the desired number of classes. The main advantage of using U-Net architecture is the lack of fully connected layers, which results in a smaller set of weights. Another advantage of the U-Net convolution network is its applicability with small training sets. Indeed, in order to train the U-Net architecture, we provided 256 by 256 textures images representative of textural classes visualized in the X-ray micro-computed tomography images with their corresponding class labels. Then, each image was tessellated into sub-regions of 32 × 32 pixels. Sub-regions were generated by

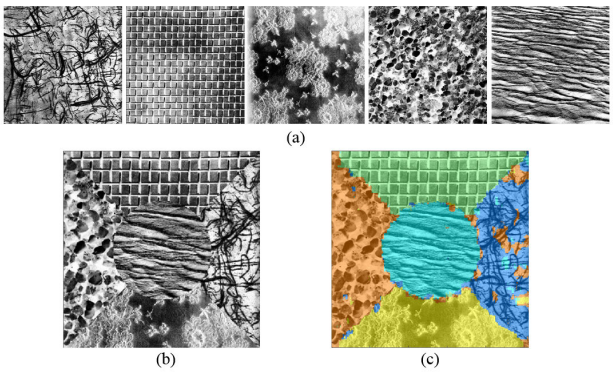

FIGURE 6. Texture classification result based on 5 Brodatz textures database: a) Input textures; b) Montage based on 5 textures; c) Classification result.

TABLE 2. Comparative accuracy (%) results of the different U-Net configurations using 3 montages of textures from Brodatz database. The highest score for each montage is highlighted in bold underline.

Method			Montage		
Layers	Optimization method	Epochs	1	2	3
10	sgdm	20	73	80	82
15	sgdm	20	84	82	77
20	sgdm	20	78	75	81
10	adam	20	79	82	82
15	adam	20	81	79	77
20	adam	20	**92**	83	72
10	RMSprop	20	81	75	81
15	RMSprop	20	87	76	73
20	RMSprop	20	77	73	75
10	adam	30	76	88	85
15	adam	30	86	**91**	86
20	adam	30	81	87	84
10	adam	50	80	82	**90**
15	adam	50	82	78	87
20	adam	50	87	85	86

shifting a 32 × 32 window vertically and horizontally in the original texture class. This procedure of traversing the image with overlap (stride = 1 pixel) allowed the creation of more than 50,000 training images without the need for an initial large database. Then, the generated dataset was split into two parts: 70% for training and 30% for testing and validation using cross validation to assess the model's performance and avoid overfitting.

We performed a pixel-based assessment, in which each correctly classified pixel was deemed "correct", and pixels that were assigned a wrong class were considered "incorrect". Figure 6 illustrates an example of textures montage from the classical Brodatz textures with the corresponding classification result for five textures. We implemented the U-Net approach by varying the number of layers, number of epochs, and optimization algorithms. The accuracy of the training set obtained was 91% using Adam optimizer. Table 2 summarizes the results obtained for the texture montage created in Figure 6.b and two additional synthetic montages of other textures from the same Brodatz database. The overall accuracy for the texture montage was around 90%.

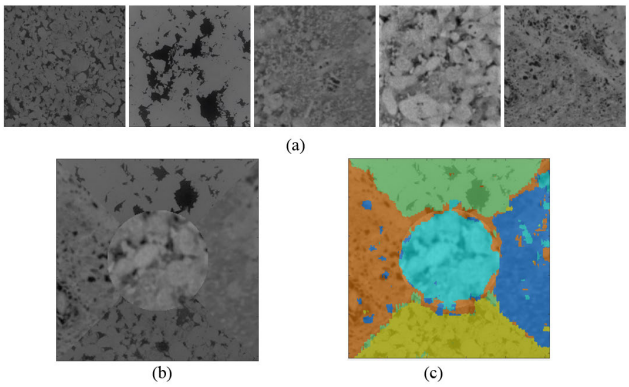

FIGURE 7. Texture classification result based on 5 textures from real X-ray Micro Computed tomography images of carbonate rock samples: a) Input textures; b) Montage based on 5 textures; c) Classification result.

In order to assess quantitatively the accuracy of the U-Net classification performance on real rock samples textures, we generated ten synthetic montages of images including five textures from X-ray micro-computed tomography images each as illustrated in Figure 7. The accuracy result of the training set was 90% while the average classification accuracy performance was around 85%. Figure 7.a shows the high quality of the classification result for real textures. Several parameters influence the quality of the results. In some cases, the highest accuracy resulted from 50 layers configurations, whereas in other textures, the best result was obtained with only 20 layers. Also, the number of epochs directly influenced the result. Indeed, on one hand, a too long training process may make the architecture too specialized. On the other hand, a too short training process may compromise the classification result. In general, we found that to obtain accuracies above 85%, the number of epochs ranged between 20 and 50 for most of X-ray micro-computed tomography images. Figure 8 shows a successful classification result for real rock texture image based on three classes identified as main representative textures.

C. MULTISCALE SIMULATION

In this section, we used texture as a vector of continuity to fill the gap between length scales. The main assumption here is that texture variability in images is directly related to rock property variability. The proposed workflow illustrated in Figure.7 began with classifying at coarse scale the sample 3D image. Based on the classification result, we extracted subsets from representative textures locations identified in the image. Then, the subsets were scanned at a higher resolution. At this fine scale, we ran numerical simulations of permeability using LBM and computed porosity using bilevel segmentation. Also, to validate the simulation results, magnified samples representing these subsets were 3D printed and their rock properties were experimentally measured. Finally, we populated the coarse scale with permeability values obtained from the fine scale and estimated the effective permeability and porosity of the sample.

At the fine scale, we used LBM as numerical method to simulate permeability. The LBM incorporates the Bhatnagar-Gross-Krook (BGK) model, and the main driving equation is expressed as a sum of steaming and colliding terms. The BGK collision operator is the most common model used to solve single fluid flow problems. The approach consider fluid as a set of particles colliding and streaming governed by the distribution function f(x,t) where x and t denote time and location of a particle, respectively (2)

$$f\,(x + e_i, t + 1) - f\,(x, t) = \Omega(x, F, \tau, t, u_i) \tag{2}$$

where ei is the particle velocity in the ith direction and τ is the relaxation time controlling the rate of approach to equilibrium. Ω is a collision operator that is required to satisfy the conservation of total mass and total momentum, and F is an external force term. The momentum density of a particle located in position x at time t is computed using the particle density function in (3):

$$\rho u\,(x) = \sum f(x) e_i \tag{3}$$

where ρ represents the density of the fluid.

Finally, we use Darcy's law, to compute absolute permeability using (4).

$$K = \frac{\mu \cdot L \cdot Q}{A \cdot \Delta P} \tag{4}$$

where K is the absolute permeability, Q is the average velocity of particles, ΔP is the gradient of pressure along a sample of length L, μ is the fluid viscosity and A is the surface area of the sample cross section.

At coarse scale, the permeability is calculated by upscaling fine scale simulations on a voxel by voxel basis, where each voxel represents a grid block of a given permeability, K(i,j,k), as described in the previous section. The index of each grid block is given by an ijk-triplet, corresponding to the three spatial dimensions x, y, and z respectively. For a single-phase flow in a porous medium, combining the continuity equation and Darcy's law in (5), leads to the Laplacian equation for the pressure in (6):

$$\nabla \cdot v = 0 \quad v = \frac{K}{\mu} \nabla p \tag{5}$$

$$\nabla \cdot \left(\frac{K}{\mu} \nabla p \right) = 0 \tag{6}$$

where v is the velocity, K is the permeability, p is the pressure and is the dynamic viscosity. Equation 6 is solved by setting the gradient pressure at the inlet and outlet of the 3D volume grid, while a no-flux Neumann condition is imposed on the other sides. Finally, the permeability is upscaled over the 3D images using two-point flux approximation for the pressure solver.

III. RESULTS AND DISCUSSION

In this section, we present results for the multiscale permeability and porosity simulation workflow using a carbonate core plug from a reservoir in the Middle East. The core

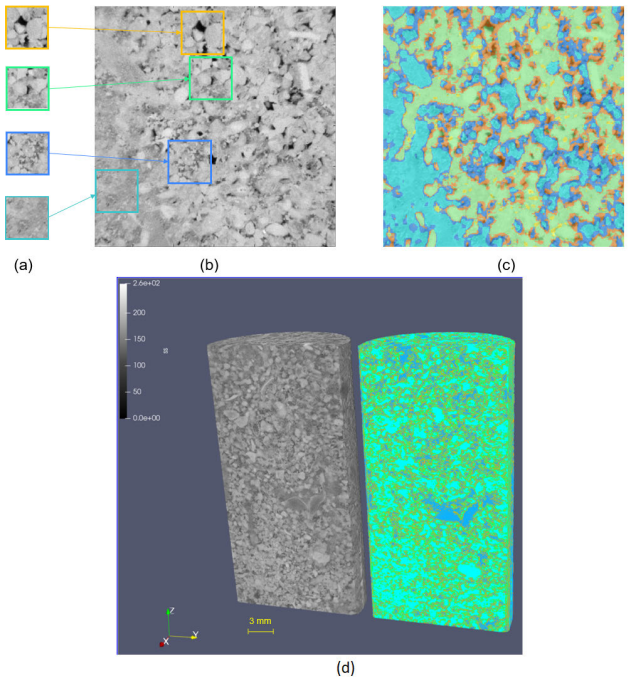

FIGURE 8. A classification result for real carbonate 3D X-ray Micro tomography image exhibiting four main representative textures: a) Identified four textures, b) Original image horizontal 2D section, c) Classified 2D image, d) classified 3D image.

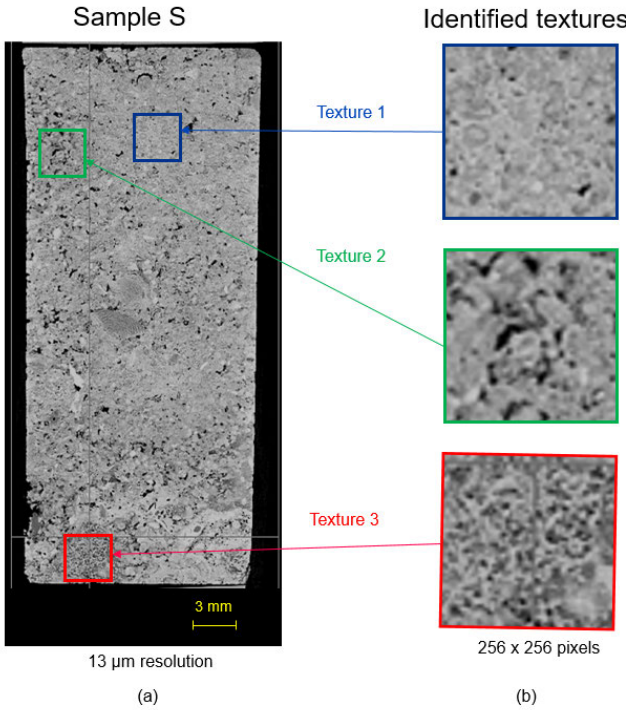

FIGURE 9. Three textures identification by a petrophysics expert from 3D X-Ray micro tomography image of the sample S: Cemented porosity (Texture 1), neomorphism (Texture2) and porous texture (Texture 3).

TABLE 3. Carbonate sample experimental properties.

	Porosity	Permeability
Dimension (mm)	Experimental (%)	Experimental (mD)
12.7	14.8	4.28

plug sample S is cylindrical with a 12.7 mm diameter and 25 mm length. We experimentally measured sample porosity and fluid permeability using the New England Research Autolab 3000/1000 (Table 3). Also, we scanned the sample at coarse scale with 13 μm resolution using a Zeiss Xradia X-ray micro-computed tomography scanner. A petrophysics expert visually identified three main textures in the sample representing cemented porosity, neomorphism and porous texture [39]. For the purposes of simplification, these textures will be called Texture 1, Texture 2 and Texture 3, respectively, as illustrated in Figure.9.

The U-Net architecture served as a supervised classification method to classify the core plug sample images into these three main classes at coarse scale. The training phase required the three identified image textures provided as 256 by 256 pixels images to the network. Several parameters were tested, including the epoch, number of layers, and optimization method, and the best results were obtained with the 20 layers configurations, an epoch value of 20, and the Adam optimization method. The result in Figure 10 shows a pixel by pixel classification based on three identified textures from the 1 centimeter diameter core plug. The training phase uses 70% of the 50,000 training images obtained by tessellation of each representative class. The accuracy result of training performance is 92% for these images. Furthermore, we generated a synthetic montage of these 3 textures and the accuracy of the classification result reached 89%. The U-Net architecture efficiently captured texture variability in the images providing an accurate pixel-by-pixel classification. This qualitative result was confirmed by visual inspection and validated by our petrophysics expert. In addition, to confirm the result quantitatively, we used a montage including the three identified textures from the rock sample studied for the upscaling procedure. The training performance was around 91% for these textures as well. The accuracy of the classification obtained for the synthetic montage of these 3 textures was around 90%.

To characterize the fine scale, we used the previous classification result to identify the location of the three representative textures, and we physically extracted 4 mm^3 subsets from each identified location. Then, we scanned each subset at 4 μm resolution as illustrated in Figure.11. At this resolution, the pore network could be identified only for Texture 2. Thus, we extracted physically smaller subsets of 1 mm^3, representative of Texture 1 and Texture 3, were extracted using a laser-cutting system and scanned at 1μm resolution as illustrated in Figure 12. We can observe some partial similarities that may exist between the two textures especially for some mineral inclusions. However, the most important

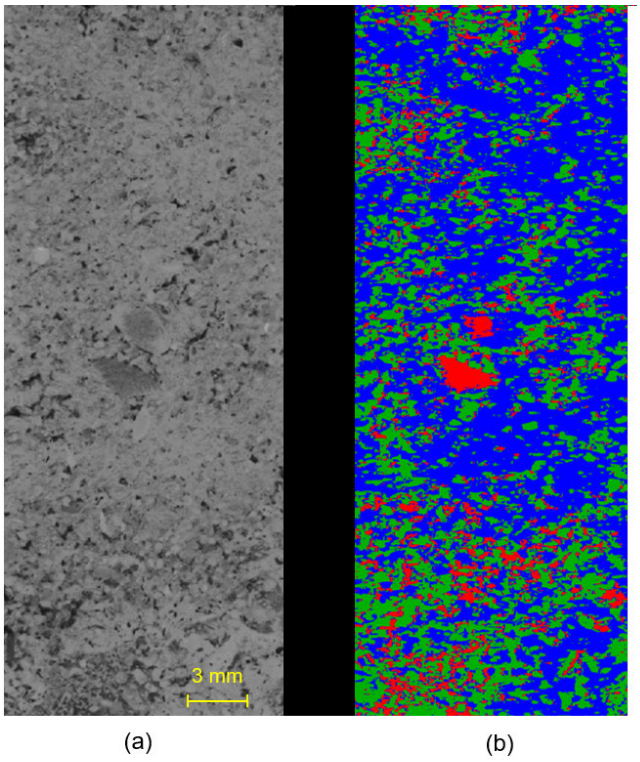

FIGURE 10. Texture classification based on the identified 3 textures for sample S. The classification result obtained using U-Net: Texture 1 in blue, Texture2 in green and Texture 3 in red.

information here is that the textural overall perceptual aspects are completely different.

In order to simulate the overall permeability of the sample, we need to estimate first the absolute permeability of each individual phase. We segmented the fine scale images of each texture using a bi-level segmentation algorithm. Then, the LBM was used to simulate the permeability representing each texture. The block size for each texture was 800^3 voxels. We used the Palabos library implementation of LBM and used 10 nodes with 12 cores each for the simulations. Permeability values for the three textures converged after 4 to 5 hours after around 200,000 iterations. The simulation results were validated by printing in 3D each representative texture and measuring the permeability values in the laboratory. Finally, we applied the effective permeability simulation method at coarse scale to obtain the simulated permeability of the whole core plug sample.

Table 4 summarizes the simulated and experimental permeability values for each texture subset and the whole sample. The effective permeability simulation at coarse scale, yielded a permeability value of 6.87 mD, when the experimental value was 4.26 mD. Also, the effective porosity for the sample S was calculated as the average of porosities assigned from fine scale to coarse scale based on the classification result. The proposed approach in this study provided a porosity of 15.6%, while the experimental measurement was 14.8%. Both simulated permeability and porosity values were in the same range as experimental properties for the

TABLE 4. Carbonate sample digital and experimental properties.

	Porosity		Permeability	
	Digital (%)	Experimental (%)	Digital (mD)	Experimental (mD)
Texture1	12.4	11.9	3.28	1.37
Texture2	17.2	16.7	357.39	128.62
Texture3	14.6	13.7	110.27	56.51
Sample S	15.6	14.8	6.87	4.28

carbonate sample S. Differences between experimental and numerical results of 3D printed samples could be caused by several sources of errors. Overall, the slight discrepancy could be attributed to three types of errors involved in the proposed workflow for the 3D print: (i) the 3D printer resolution limitation, (ii) image processing with segmentation, (iii) experimental measurement in the lab.

The first source of error is the limitation of the printer resolution. Indeed, any pore structure in the same range printer resolution could produce non-smooth surfaces or closed pores that cannot be cleaned. This may reduce porosity and permeability values as observed in the results. The second source of error is related to the accuracy of segmentation method and numerical simulation applied at fine scale. Nevertheless, these two processes are applied at highest resolution which makes the impact of this error quite moderate. The third source of error is related to the laboratory measurement setup. Even though we repeated permeability measurements for all studied samples these values are subject to variations as reported with error bars in Figure 3.c.

One major advantage of using texture classification is the automated selection of representative subsets locations. This step reduces sensitivity to the operator manual selection, which could be subjective or approximate. Indeed, the results of this study demonstrate that even with very small numbers of images the U-Net can be trained, and accurate classification of the main representative textures can be obtained. Another advantage is that the automated upscaling method uses texture as a vector of continuity to fill the gap between length scales. In this particular application, three textures were identified, but the same model can be generalized to a larger number of classes. Indeed, the accuracy of the proposed classification approach is greater than 85% for most textures representing real rock samples that were tested. An additional advantage of this approach is that the method can be reproduced at coarser length scales if needed, assuming the existence of textural variability in the images.

Although the proposed textural classification method provided quantitative accurate results, the workflow may suffer from the subjective step in which the representative textural classes are selected. In order to overcome this limitation, future study could incorporate unsupervised approaches to automatically capture the most representative classes and

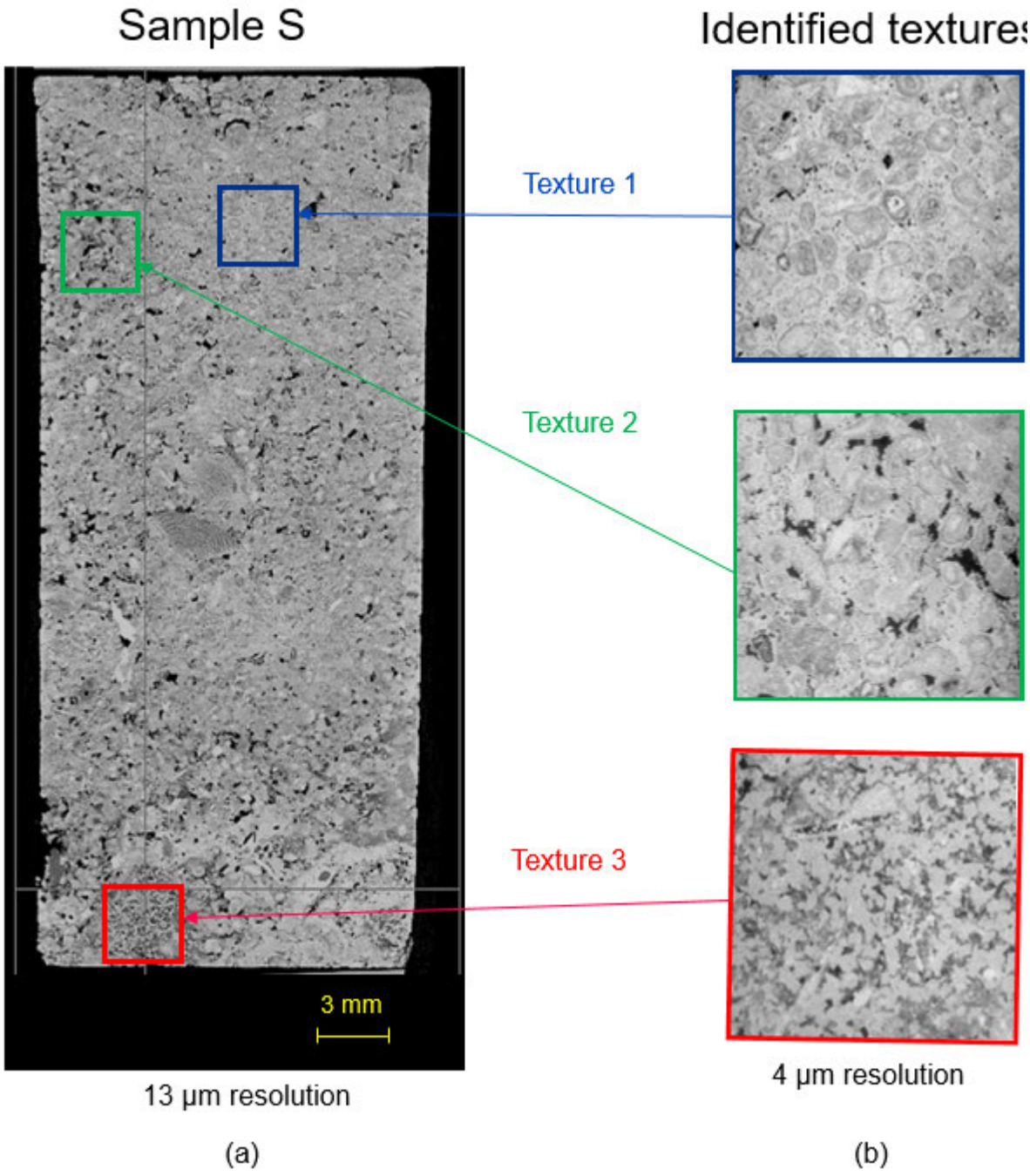

FIGURE 11. Three textures identified and scanned at fine scale.

then classify the 3D image. Moreover, the use of 3D printing in our proposed workflow aimed to experimentally validate the numerical simulations run at fine scale. Experimental procedures involved in 3D printing and cleaning are quite sensitive and are time- consuming. This approach can be considered as a validation step and, thus, will not be needed for the upscaling workflow in future validation studies. Indeed, results obtained in Table 4 shows that the permeability simulation results obtained through LBM align with the experimental measurements of each 3D printed textures. This result confirms that LBM is an accurate and reliable numerical simulation tool to simulate permeability even in a complex pore network of carbonate samples.

It is worth mentioning that we tested the entire workflow on a heterogeneous carbonate sample with complex pore spaces exhibiting high variability in permeability (1.37-110mD). However, the comprehensive approach can be applied to any samples and allows for experimental verification at core

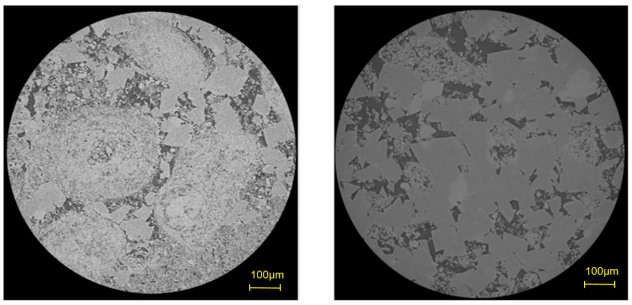

FIGURE 12. 2D slices from Xray Micro tomography images of 1 mm diameter subsets scanned at high resolution (1μm); a) Subset representing Texture 1; b) Subset representing Texture 3.

size in contrast to recent studies [40], [41], only relevant at pore scale. Overall, our workflow allowing to bridge the gap between pore and core scale can be an attractive tool to expand the use of DRP.

IV. CONCLUSION

This study proposed a novel upscaling method to simulate porosity and permeability in carbonate rock samples based on machine learning. We used U-Net architecture as a CNN tool to classify textures at coarse scale and target the position of subsets to be physically extracted at fine scale. Fine-scale rock properties were numerically simulated, and the 3D printing technique magnified subsets and to experimentally validate the simulation results. Finally, we upscaled rock properties from fine scale to coarse scale using the texture classification result. We implemented the approach on a real carbonate core plug sample from the Middle East and obtained accurate results when compared to the experimental measurements. Although this approach provided relevant and accurate results in this study, more samples should be validated for better quantitative estimation of petrophysical properties at core scale. The study revealed also that the quantitative textural description allowed the identification of multiple REV's for the permeability in terms of texture units to characterize carbonate samples. The approach is subject to several challenges. Indeed, the method works only if we can capture variability of textures in the images. In addition, the classification is currently 2D, whereas the data is 3D. A direct 3D classification should be developed to use the full spatial information. In a future study, we will explore the use of non-supervised methods in order to fully automate the texture classification procedure.

ACKNOWLEDGMENT

The authors would like to thank Halliburton Abu Dhabi and 3D Vinci Creation Dubai for the fruitful discussions and collaboration for data acquisition.

REFERENCES

[1] C. Hollis, V. Vahrenkamp, S. Tull, A. Mookerjee, and C. Taberner, "Pore system characterisation in heterogeneous carbonates: An alternative approach to widely-used rock-typing methodologies," *Mar. Petroleum Geol.*, vol. 27, no. 4, pp. 772–793, 2010, doi: 10.1016/j.marpetgeo.2009.12.002.

[2] M. R. Dernaika, B. Mansour, D. Gonzalez, S. Koronfol, F. Mahgoub, O. Al Jallad, and M. Contreras, "Upscaled permeability and rock types in a heterogeneous carbonate core from the Middle East," *Soc. Petroleum Eng.*, to be published, doi: 10.2118/185991-MS.

[3] C. H. Arns, F. Bauget, and A. Limaye, "Pore scale characterization of carbonates using X-ray microtomography," *Soc. Petroleum Eng. J.*, vol. 10, no. 4, pp. 475–484, 2005, doi: 10.2118/90368-PA.

[4] M. S. Jouini and S. Vega, "Simulation of elastic properties in carbonates," *Lead. Edge*, vol. 30, no. 12, pp. 1400–1407, Dec. 2011, doi: 10.1190/1.3672485.

[5] H. Andra, N. Combaret, and J. Dvorkin, "Digital rock physics benchmarks—Part I: Imaging and segmentation," *Comput. Geosci.*, vol. 50, pp. 25–32, Jan. 2013, doi: 10.1016/j.cageo.2012.09.005.

[6] Y.-Z. Hsieh, M.-C. Su, J.-H. Chen, B. A. Badjie, and Y.-M. Su, "Developing a PSO-based projection algorithm for a porosity detection system using X-ray CT images of permeable concrete," *IEEE Access*, vol. 6, pp. 64406–64415, 2018, doi: 10.1109/ACCESS.2018.2877157.

[7] M. S. Jouini and N. Keskes, "Numerical estimation of rock properties and textural facies classification of core samples using X-ray computed tomography images," *Appl. Math. Model.*, vol. 41, pp. 562–581, Jan. 2017, doi: 10.1016/j.apm.2016.09.021.

[8] M. Tembely, A. AlSumaiti, M. Jouini, and K. Rahimov, "The effect of heat transfer and polymer concentration on non-newtonian fluid from pore-scale simulation of rock X-ray micro-CT," *Polymers*, vol. 9, no. 12, p. 509, Oct. 2017, doi: 10.3390/polym9100509.

[9] J. E. McClure, Z. Li, M. Berrill, and T. Ramstad, "The LBPM software package for simulating multiphase flow on digital images of porous rocks," *Comput. Geosci.*, vol. 25, no. 3, pp. 871–895, Jun. 2021, doi: 10.1007/s10596-020-10028-9.

[10] M. S. Jouini, F. Umbhauer, J. P. Leduc, and N. Keskes, "Petrophysical properties prediction using 3D core scanner imagery," in *Proc. Soc. Petroleum Eng. Conf.*, Denver, CO, USA, 2008, doi: 10.2118/116393-MS.

[11] A. S. Grader, A. B. S. Clark, T. Al-Dayyani, and A. Nur, "Computations of porosity and permeability of sparic carbonate using multi-scale CT images," presented at the Int. Symp. Soc. Core Analysist Held, Noordwijk, The Netherlands, Sep. 2009.

[12] M. S. Jouini, S. Vega, and A. Al-Ratrout, "Numerical estimation of carbonate rock properties using multiscale images," *Geophys. Prospecting*, vol. 63, no. 2, pp. 405–421, Mar. 2015, doi: 10.1111/1365-2478.12156.

[13] T. F. Faisal, A. Awedalkarim, S. Chevalier, M. S. Jouini, and M. Sassi, "Direct scale comparison of numerical linear elastic moduli with acoustic experiments for carbonate rock X-ray CT scanned at multi-resolutions," *J. Petroleum Sci. Eng.*, vol. 152, pp. 653–663, Apr. 2017, doi: 10.1016/j.petrol.2017.01.025.

[14] R. Sok, T. Varslot, and A. Ghous, "Pore scale characterization of carbonates at multiple scales: Integration of micro-CT, BSEM, and FIBSEM," *Petrophysics*, vol. 51, no. 6, pp. 379–387, 2010.

[15] Z. Jiang, M. I. J. van Dijke, K. S. Sorbie, and G. D. Couples, "Representation of multiscale heterogeneity via multiscale pore networks," *Water Resour. Res.*, vol. 49, no. 9, pp. 5437–5449, Sep. 2013, doi: 10.1002/wrcr.20304.

[16] A. D. Khalili, J.-Y.-Y. Arns, F. Hussain, Y. Cinar, W. V. V. Pinczewski, and C. H. H. Arns, "Permeability upscaling for carbonates from the pore scale by use of multiscale X-ray-CT images," *SPE Reservoir Eval. Eng.*, vol. 16, no. 04, pp. 353–368, Nov. 2013, doi: 10.2118/152640-PA.

[17] R. Sungkorn, M. Anyela, and G. Carpio, "Multi-scale and upscaling of digital rock physics with a machine that can learn about rocks," in *Proc. Int. Symp. Soc. Core Analysts*, 2015, pp. 16–21.

[18] A. Islam, T. F. Faisal, S. Chevalier, M. S. Jouini, and M. Sassi, "Multi-scale experimental and numerical simulation workflow of absolute permeability in heterogeneous carbonates," *J. Petroleum Sci. Eng.*, vol. 173, pp. 326–338, Feb. 2019, doi: 10.1016/j.petrol.2018.10.031.

[19] M. J. Munawar, S. Vega, C. Lin, M. Alsuwaidi, N. Ahsan, and R. R. Bhakta, "Upscaling reservoir rock porosity by fractal dimension using three-dimensional micro-computed tomography and two-dimensional scanning electron microscope images," *J. Energy Resour. Technol.*, vol. 143, no. 1, p. 143, Jan. 2021, doi: 10.1115/1.4047589.

[20] C. Bouman and B. Liu, "Multiple resolution segmentation of textured images," *IEEE Trans. Pattern Anal. Mach. Intell.*, vol. 13, no. 2, pp. 99–113, Feb. 1991, doi: 10.1109/34.67641.

[21] A. K. Jain and F. Farrokhnia, "Unsupervised texture segmentation using Gabor filters," *Pattern Recognit.*, vol. 24, no. 12, pp. 1167–1186, 1991, doi: 10.1016/0031-3203(91)90143-S.

[22] E. A. Hoffman, J. M. Reinhardt, M. Sonka, B. A. Simon, J. Guo, O. Saba, D. Chon, S. Samrah, H. Shikata, and J. Tschirren, "Characterization of the interstitial lung diseases via density-based and texture-based analysis of computed tomography images of lung structure and function," *Academic Radiol.*, vol. 10, no. 10, pp. 1104–1118, 2003, doi: 10.1016/S1076-6332(03)00330-1.

[23] C. C. Reyes-Aldasoro and A. Bhalerao, "Volumetric texture description and discriminant feature selection for MRI," in *Information Processing in Medical Imaging*, C. Noble, Ed. Ambleside, U.K.: Taylor, 2003, pp. 282–293, doi: 10.1007/978-3-540-45087-0_24.

[24] R. M. Haralick, "Statistical and structural approaches to texture," *Proc. IEEE*, vol. 67, no. 5, pp. 786–804, May 1979, doi: 10.1109/PROC.1979.11328.

[25] J. Portilla and E. P. Simoncelli, "A parametric texture model based on joint statistics of complex wavelet coefficients," *Int. J. Comput. Vis.*, vol. 40, no. 1, pp. 49–71, Oct. 2000, doi: 10.1023/A:1026553619983.

[26] C. C. Reyes-Aldasoro and A. Bhalerao, "The bhattacharyya space for feature selection and its application to texture segmentation," *Pattern Recognit.*, vol. 39, no. 5, pp. 812–826, May 2006, doi: 10.1016/j.patcog.2005.12.003.

[27] M. Prasad and T. Mukerji, "Analysis of microstructural textures and wave propagation characteristics in shales," in *Proc. SEG Tech. Program Expanded Abstr.*, Dallas, TX, USA, Jan. 2003, pp. 1648–1651, doi: 10.1190/1.1817620.

[28] M. Knackstedt, K. J. Saadatfar, and M. Senden, "Rock fabric and texture from digital core analysis," in *Proc. 46th Annu. Logging Symp. Soc. Petrophysicists Well-Log Analysts (SPWLA)*, New Orleans, LA, USA, 2005.

[29] M. S. Jouini, A. AlSumaiti, M. Tembely, F. Hjouj, and K. Rahimov, "Permeability upscaling in complex carbonate samples using textures of micro-computed tomography images," *Int. J. Model. Simul.*, vol. 40, no. 4, pp. 245–259, Jul. 2020, doi: 10.1080/02286203.2019.1596728.

[30] O. Ronneberger, P. Fischer, and T. Brox, "U-Net: Convolutional networks for biomedical image segmentation," in *Medical Image Computing and Computer-Assisted Intervention–(MICCAI)*. vol. 9350. Berlin, Germany: Springer, Oct. 2015, pp. 234–241, doi: 10.1007/978-3-319-24574-4_28.

[31] T. Falk, D. Mai, R. Bensch, Ö. Çiçek, and A. Abdulkadir, "U-Net: Deep learning for cell counting, detection, and morphometry," *Nature Methods*, vol. 16, no. 1, p. 67, 2018, doi: 10.1038/s41592-018-0261-2.

[32] C. Zhang, X. Song, and L. Azevedo, "U-net generative adversarial network for subsurface facies modeling," *Comput. Geosci.*, vol. 25, no. 1, pp. 553–573, Feb. 2021, doi: 10.1007/s10596-020-10027-w.

[33] A. Eshghinejadfard, L. Daróczy, G. Janiga, and D. Thévenin, "Calculation of the permeability in porous media using the lattice Boltzmann method," *Int. J. Heat Fluid Flow*, vol. 62, pp. 93–103, Dec. 2016.

[34] J. A. White, R. I. Borja, and J. T. Fredrich, "Calculating the effective permeability of sandstone with multiscale lattice Boltzmann/finite element simulations," *Acta Geotechnica*, vol. 1, no. 4, pp. 195–209, Nov. 2006, doi: 10.1007/s11440-006-0018-4.

[35] C. Karabağ, J. Verhoeven, N. R. Miller, and C. C. Reyes-Aldasoro, "Texture segmentation: An objective comparison between five traditional algorithms and a deep-learning U-Net architecture," *Appl. Sci.*, vol. 9, no. 18, p. 3900, Sep. 2019, doi: 10.3390/app9183900.

[36] D. Head and T. Vanorio, "Effects of changes in rock microstructures on permeability: 3-D printing investigation," *Geophys. Res. Lett.*, vol. 43, p. 7494 7502, 2016, doi: 10.1002/2016GL069334.

[37] S. Ishutov, T. D. Jobe, S. Zhang, M. Gonzalez, S. M. Agar, F. J. Hasiuk, F. Watson, S. Geiger, E. Mackay, and R. Chalaturnyk, "Three-dimensional printing for geoscience: Fundamental research, education, and applications for the petroleum industry," *AAPG Bull.*, vol. 102, no. 1, pp. 1–26, Jan. 2018.

[38] H. Vogel and A. Kretzschmar, "Topological characterization of pore space in soil—Sample preparation and digital image-processing," *Geoderma*, vol. 73, pp. 23–38, Sep. 1996, doi: 10.1016/0016-7061(96)00043-2.

[39] J. A. D. Dickson, "Neomorphism and recrystallization," in *Encyclopedia of Sediments and Sedimentary Rocks*. (Encyclopedia of Earth Sciences Series). Dordrecht, The Netherlands: Springer, 1978, doi: 10.1007/978-1-4020-3609-5_143.

[40] O. Sudakov, E. Burnaev, and D. Koroteev, "Driving digital rock towards machine learning: Predicting permeability with gradient boosting and deep neural networks," *Comput. Geosci.*, vol. 127, pp. 91–98, Jun. 2019, doi: 10.1016/j.cageo.2019.02.002.

[41] J. Wu, X. Yin, and H. Xiao, "Seeing permeability from images: Fast prediction with convolutional neural networks," *Sci. Bull.*, vol. 63, no. 18, pp. 1215–1222, Sep. 2018, doi: 10.1016/j.scib.2018.08.006.

MOHAMED SOUFIANE JOUINI received the M.E. degree in electrical engineering from the École Nationale Supérieure d'Électrotechnique, d'Électronique, d'Informatique, d'Hydraulique et des Télécommunications, Toulouse, France, in 2004, the M.S. degree in signal and image processing from the National Polytechnic Institute of Toulouse, France, in 2005, and the Ph.D. degree in signal and image processing from the University of Bordeaux, France, in 2009. From 2009 to 2010, he was a Research Scientist with SAGEM MORPHO, Paris, France. Then, he was a Research Scientist with the Petroleum Institute, Abu Dhabi, United Arab Emirates. In 2014, he was promoted as an Assistant Professor and then in 2020 an Associate Professor with the Department of Applied Mathematics, Khalifa University, Abu Dhabi.

JORGE SALGADO GOMES has more than 30 years of industry experience. He is currently the Head of the Discipline, Geoscience Subsurface Excellence Division, Abu Dhabi National Oil Company. Previously, he was occupying the PARTEX Chaired Professor position of petroleum engineering with the Khalifa University Petroleum Institute, Abu Dhabi.

MOUSSA TEMBELY is currently a Research Scientist with Khalifa University. He is also an expert in numerical simulation in porous media. Previously, he worked with Concordia University, Montreal, QC, Canada, as a Researcher of mathematical physics, computational physics and fluid dynamics.

EZDEEN RAED IBRAHIM is currently pursuing the M.Sc. degree with the Department of Petroleum Geosciences, Khalifa University.